Theor Chem Acc (2003) 110: 307–321
DOI 10.1007/s00214-003-0504-9

Theoretical
Chemistry Accounts

Feature article

Electronic coupling in electron transfer and the influence of nuclear modes: theoretical and computational probes

Marshall D. Newton

Department of Chemistry, Brookhaven National Laboratory, Upton, NY11973, USA

Received: 30 March 2003 / Accepted: 2 July 2003 / Published online: 13 November 2003

Abstract. Long-range electronic coupling of local donor and acceptor sites is formulated in the context of thermal and optical electron transfer and then illustrated with examples based on electronic structure calculations. The relationship of the calculated results to available experimental kinetic and optical data is discussed in detail. The influence of nuclear modes on the magnitude of the coupling (i.e., departures from the Condon approximation) is investigated in terms of both discrete molecular modes and solvent modes, and a general expression is presented for the modulation of the superexchange tunneling gap by motion along the electron transfer reaction coordinate.

Keywords: Electron transfer – Electronic coupling matrix element – Condon approximation – Reaction Coordinate – Reorganization energy

Introduction

Long-range electron transfer (ET) between local donor (D) and acceptor (A) sites (e.g., charge separation, CS, of the type $DA \rightarrow D^{+}A^{-}$) is of central importance in many areas of chemistry and related disciplines [1, 2, 3, 4, 5, 6, 7, 8, 9, 10, 11,12, 13]. A continuing challenge for theoretical chemistry is the need to characterize the factors controlling the strength of D/A coupling and its quantitative role in the mechanism of overall ET kinetics [7, 8, 9]. ET occurs in a rich variety of contexts: thermal and optical, intramolecular and intermolecular, homogeneous and interfacial. ET kinetics between discrete D and A sites is also closely related to electronic transport in conductive junctions [3]. The field of ET is especially attractive for theoretical study because of the availability of unified theories which may be readily adapted to the many variants noted earlier.

The focus of the present work is the strength of D/A coupling, as represented by the effective Hamiltonian matrix element, H_{DA}. Before proceeding to the details of H_{DA}, however, we first establish the kinetic context by presenting some standard models for ET rate constants, k_{ET}, in the limit of nonadiabatic ET, noting also various extensions of theory which may be required to accommodate ET processes of current experimental interest. We then discuss, the formulation of the space of electronic states needed to represent an ET process and the specification of states within this space. In the remaining sections, specific expressions for H_{DA} and the factors controlling its magnitude are analyzed and illustrated in terms of the results of sample calculations. These factors include the chemical, geometrical and electronic structure of the "solute" DBA (comprising the D and A groups and any intervening "bridge", B) and the response of the surrounding medium ("solvent").

Kinetic context

The ET rate constant, k_{ET}, is determined by the energetics of the ET system and the strength of D/A electronic coupling (H_{DA}). The energetics and the coupling may be linked in varying degrees through their joint dependence on the nuclear modes of the solute and surrounding medium. The coupling of solute and medium is often assumed to be linear; however, the consequences of nonlinearity can be significant [12, 14, 15]. Matyushov and Voth [14] have shown recently that nonlinear coupling (due, for example, to distinct initial and final state solute polarizabilities, α) may have an appreciable qualitative as well as quantitative influence on ET kinetics and associated aspects of optical ET lineshapes, and they have provided compact new models which take account of the nonlinear behavior.

Correspondence to: M. D. Newton
e-mail: newton@bnl.gov

Matyushov and Newton [15] have discussed the role of nonlinearity arising from the combined effects of polarizability shifts and delocalization of initial and final states in controlling the solvent dependence of optical ET lineshapes for coumarin-153. In the present account, with focus on D/A coupling, we do not explicitly consider nonlinear effects (although the detailed electronic structure calculations involving solvation do not impose strict linearity), choosing rather to illustrate some important concepts in terms of linear models. Reference to the role of solute polarizability is made, however, in Sects. 3 and 6 in connection with analysis of the influence of solvent on H_{DA} magnitudes.

To provide a point of reference for appreciating the kinetic role of H_{DA}, we consider a useful limiting expression for k_{ET} which is valid for thermal ET within the nonadiabatic (weak D/A coupling) transition-state approximation in the case of classical (high-temperature) harmonic nuclear motion [4, 5, 6, 7, 8]:

$$k_{ET} = \left(2\pi H_{DA}^2/\hbar\right)\Big/(4\pi\lambda k_B T)^{1/2}\left[\exp-\left(\Delta G^{\dagger}\Big/k_B T\right)\right], \tag{1}$$

$$\Delta G^{\dagger} = \left(\Delta G^0 + \lambda\right)^2\Big/4\lambda. \tag{2}$$

The form of Eq. (2) is easily extended to the case of optical ET [10].

Equations (1) and (2) highlight the central importance of two free-energy quantities (the reaction exothermicity, ΔG^0, and the reorganization energy, λ) and the coupling element H_{DA}. The activation free energy, $\Delta G^{\dagger}$, is related to ΔG^0 by the well-known Marcus quadratic free-energy expression (Eq. 2) [11]. Equation (1) superficially resembles an Arrhenius rate constant expression, with a Boltzmann activation factor and a prefactor (the first two factors in Eq. 1), which displays only weak temperature dependence ($T^{-1/2}$). Note, however, that any entropic contributions to $\Delta G^{\dagger}$ belong properly to the Arrhenius prefactor, a situation which must be taken into account in attempts to extract H_{DA} values from experimental prefactors [12]. In spite of the deceptively simple factorizable form of k_{ET} in Eq. (1), H_{DA} and $\Delta G^{\dagger}$ are not necessarily fully independent quantities, as noted earlier, and some of their possible interrelationships will be examined later. H_{DA}, of course, implies a particular pair of states, the initial and final "diabatic" states in a thermal ET process [8]. We defer the discussion of this topic until the next section.

Energetics due to nuclear modes

In the classical limit for nuclear motion (Eq. 1) all nuclear modes are treated on the same (high-temperature) footing. It is often desirable to separate the modes into low-frequency and high-frequency sets, treated, respectively, classically ($h\nu \ll k_B T$) and quantum mechanically ($h\nu \gtrsim k_B T$), where ν is the frequency of a given mode. For separable coordinates (e.g., harmonic oscillators) the total reorganization λ may be expressed as the sum

$$\lambda = \lambda^{lf} + \lambda^{hf}, \tag{3}$$

where in general λ^{lf} and λ^{hf} may each have significant contributions from both solute (i.e., the DBA system) and medium modes. Typically, however, λ^{lf} and λ^{hf} are dominated, respectively, by medium (or solvent) and solute (so-called inner-shell) modes, and in the following, we use the notation $\lambda^s \equiv \lambda^{lf}$ and $\lambda^{in} \equiv \lambda^{hf}$. Reorganization energy is the consequence of a shift in equilibrium coordinates in the course of an ET process. For a discrete harmonic mode, q, with force constant k_q and shift Δq,

$$\lambda_q = k_q(\Delta q)^2\Big/2. \tag{4}$$

The analog for continuum polarization medium modes has been given by Marcus [11]:

$$\lambda_s = (1/\varepsilon_\infty - 1/\varepsilon_0)(1/8\pi)\int_{V_s}|\bar{D}(\Delta\rho)|^2 d^3r, \tag{5}$$

where ε_∞ and ε_0 are the optical and static medium dielectric constants, V_s is the volume occupied by the medium, and **D** is the electric displacement vector, taken as a linear functional of the shift in solute charge density ($\Delta\rho$) in the ET process. The Franck–Condon control of nonadiabatic ET leads to the activation energy $\Delta G^{\dagger}$ given in Eq. (3), the height of the minimum-energy crossing point of the initial and final state energies in the harmonic approximation, relative to the initial state minimum energy.

We now represent the energetics relevant to ET in terms of energy profiles for initial and final diabatic states along a reaction coordinate, as illustrated in Fig. 1 for several types of ET (or hole transfer, HT) process, both thermal and optical. The distinction between ET and HT is considered later. These free-energy surfaces serve as effective potential-energy surfaces, V_i (initial) and V_f (final) [13]:

$$V_i = <\mathbf{q}|\mathbf{K}|\mathbf{q}>/2, \tag{6a}$$

$$V_f = <\mathbf{q} - \Delta\mathbf{q}|\mathbf{K}|\mathbf{q} - \Delta\mathbf{q}>/2 + \Delta G^0, \tag{6b}$$

where the vector $|\mathbf{q}>$ (and its equilibrium shift, $|\Delta\mathbf{q}>$) includes all the harmonic modes, and **K** is the force constant matrix. In this notation,

$$\lambda = <\Delta\mathbf{q}|\underline{\mathbf{K}}|\Delta\mathbf{q}>/2. \tag{7}$$

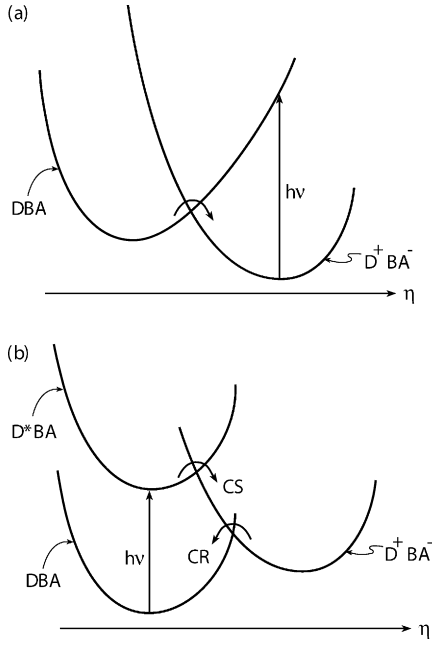

Fig. 1. a Schematic representation of optical and thermal electron transfer (*ET*), corresponding, respectively, to the vertical transition with excitation energy *hν* and passage through the transition-state (or crossing) region. **b** Sequence of photoinitiated ET charge separation (*CS*) from a locally excited state, followed by charge recombination (*CR*) back to the ground state. The CS,CR notation is generally limited to cases where the donor (*D*) and acceptor (*A*) sites are initially charge neutral (as drawn)

Formally, Eqs. (6a, 6b) and (7) can be understood to include both the discrete and the continuum modes discussed previously. The quantity which controls the ET kinetics is the vertical energy gap between V_i and V_f, and we adopt this as the reaction coordinate, η (see also Refs. [13, 16]):

$$\eta = V_f - V_i = -<\Delta\mathbf{q}|\mathbf{K}|\mathbf{q}> + \lambda + \Delta G^0. \tag{8}$$

If we define the minimum-energy value of V_i in q space (at $|\mathbf{q}> = |\mathbf{q}_{\min}(\eta)>$), subject to the constraint of a particular value of η, a straight-line path lying along the $|\Delta\mathbf{q}>$ direction is obtained [8],

$$\left|\mathbf{q}_{\min}(\eta)\right> = \left[\left(\lambda + \Delta G^0 - \eta\right)/2\lambda\right]\left|\Delta\mathbf{q}\right>. \tag{9}$$

Along this path, V_i and V_f may be re-expressed as harmonic functions of the single coordinate η:

$$V_i = \left(\lambda + \Delta G^0 - \eta\right)^2 \Big/ 4\lambda, \tag{10}$$

$$V_f = \left(\lambda - \Delta G^0 + \eta\right)^2 \Big/ 4\lambda + \Delta G^0. \tag{11}$$

Any linear function of η can serve equally well as a reaction coordinate as long as all the coordinates contributing to the collective coordinate η are globally harmonic (i.e., with the same force constant matrix for initial and final states, as in Eq. 7). Even in the non-harmonic case, one may still define η as the vertical energy gap $V_f - V_i$, but η will no longer be linear in $|\mathbf{q}>$, in contrast to Eq. (8). In this case (discussed in detail in Ref. [14]), V_i and V_f are not quadratic in η, but the relationship noted by Tachiya [17],

$$V_f(\eta) = V_i(\eta) + \eta, \tag{12}$$

remains valid in general, indicating clearly that at a given value of η, V_i and V_f have the same curvature with respect to η, irrespective of the functional form of V_i and V_f.

Extension of the classical nonadiabatic transition-state theory framework

The activation free energy $\Delta G^\dagger$ in the classical harmonic case (Eq. 2) corresponds to V_i at the diabatic crossing (see examples in Fig. 1), where $\eta = \eta^\dagger = 0$. Equation (1), which treats the transferring electron quantum mechanically (as reflected by the matrix element H_{DA}, sometimes described as a manifestation of "electron tunneling"), may also be extended to include quantal nuclear modes. One approach maintains the form of Eq. (1) but employs semiclassical generalizations of $\Delta G^\dagger$ and the prefactor [18]. A popular current approach due to Jortner and Bixon [19] uses another semiclassical model, in which specific vibronic analogs of Eq. (1), k_{vw}, are superposed,

$$k_{ET} = \sum_{v,w} P_v\, k_{vw}, \tag{13}$$

where v and w are the initial and final vibronic quantum states (products of electronic and harmonic vibrational states) and P_v is the probability for initial state v (e.g., given by a Boltzmann factor for a thermally equilibrated initial state); k_{vw} is obtained from the classical expression (Eq. 1) by the following transformations [19]:

$$H_{DA}^2 \rightarrow H_{DA}^2 S_{vw}, \tag{14a}$$

$$\lambda \rightarrow \lambda^S, \tag{14b}$$

$$\Delta G^0 \rightarrow \Delta G^0_{v,w} = \Delta G^0 + \Delta n_{vw}(h\nu), \tag{14c}$$

where S_{vw} is a vibrational Franck–Condon factor and Δn_{vw} is the change in vibrational quantum number, n, in the ET process (in Eq. 14c we assume a single effective quantum mode with frequency ν; in this case, S_{vw} depends on the parameter $\lambda_{in}/h\nu$) [19].

The right-hand side of Eq. (14a) implies the Condon approximation [20], in which a fixed value of H_{DA} is factored out of the full vibronic matrix element. For thermal ET, H_{DA} should be evaluated at the transition-state configuration of the system. In the classical limit, this occurs at the minimum-energy diabatic crossing point, $\eta^{\dagger}$ (Fig. 1). When nuclear tunneling is present, the reaction is not confined to a single point along η, and a suitable root-mean-square value of H_{DA} may be employed as an alternative to evaluating H_{DA} at $\eta^{\dagger}$. Some examples of non-Condon behavior are considered later. Equation (13) lacks the transparent Arrhenius-like structure of Eq. (1), but of course may be subjected to Arrhenius analysis, yielding an activation energy which reflects a reduced barrier (relative to the classical limit) due to nuclear tunneling. However, for tunneling at finite temperatures this effect is somewhat offset by a negative effective activation entropy in the prefactor [21].

Returning to the classical nuclear model given by Eq. (1), we note that the prefactor may be recast as $(\kappa_{el})(\nu_{eff})$, where κ_{el} is the electronic transmission factor and ν_{eff} is the frequency of the effective mode which carries the system through the crossing at the transition state [8, 18]. In the nonadiabatic limit (Eq. 1), $\kappa_{el} \ll 1$. As the coupling element H_{DA} increases in magnitude (other quantities being kept constant), the adiabatic limit within the transition-state theory (TST) framework will eventually be reached ($\kappa_{el} \sim 1$), as may be described, for example, in terms of the Landau–Zener model [21]. However, the "degree of adiabaticity" is clearly a joint property of several parameters (i.e., λ, ν_{eff}, and T as well as H_{DA}). Furthermore, as nuclear tunneling is introduced, effective coupling elements will tend to be reduced in magnitude (e.g., as in Eq. 14a, where $S_{vw} \leq 1$), thus bringing the ET process closer to the nonadiabatic limit [8, 19]. On the other hand, when the adiabatic limit is approached, some diffusional process (e.g., solvent dynamics) may become the rate-determining step, thus requiring one to go beyond the TST [7, 8, 19]. A further point to note is that as H_{DA} increases in magnitude, the adiabatic barrier height will be reduced as a result of avoided crossing at the transition state; for example, for a thermoneutral process ($\Delta G^0 = 0$), we find [18]

$$\Delta G^{\dagger} = \lambda/4 - |H_{DA}| + H_{DA}^2/\lambda . \tag{15}$$

The variation of k_{ET} with D/A separation, r_{DA}, is of great mechanistic interest [1, 2, 3, 4, 5, 6, 7, 8, 9]. Primary focus is usually placed on the expected (see later) exponential decay of H_{DA} with respect to r_{DA}. However, intersite Coulombic contributions to ΔG^0 may also have a significant influence on the r_{DA} dependence of k_{ET}, a factor which must be carefully taken into account in analysis of experimental kinetic data [22, 23]. Furthermore, r_{DA} must be recognized as an effective quantity with no unique definition [8]. The next section offers a theoretical definition based on the centroids of the D and A states in a given ET process.

Finally, we note that in contrast to the mechanism embodied in Eq. (1), in which B-mediated electron (or hole) tunneling occurs directly from the D to the A site, alternative sequential mechanisms are possible, in which shorter electron tunneling steps involving the temporary occupation of intermediate B sites by the transferring electron are linked by overall diffusive hopping, thus yielding a relatively weak overall dependence of k_{ET} on r_{DA} [24].

Electronic spaces and states

The foregoing discussion of ET kinetics presumes a knowledge of the relevant electronic states, either the charge-localized initial and final diabatic states, the DBA, $D^{+}BA^{-}$, etc., "valence-bond structures" introduced earlier, or the corresponding adiabatic states, the eigenstates of the electronic Hamiltonian. In typical situations, the diabatic states are the natural basis for treating thermal ET, whereas the adiabatic states, coupled by the transition dipole moment, are employed for analysis of optical ET [8, 25]. Owing to mixing via H_{DA}, the adiabatic and diabatic energy profiles will be distinct, an effect suppressed for simplicity in Fig. 1.

We now consider electronic spaces spanned by eigenstates of the electronic Hamiltonian. The minimum-state space suitable for representing one or more thermal ET processes of interest is one which provides an adequate basis for the relevant charge-localized diabatic states (represented by the abbreviated D, A notation). As a physically appealing, operational definition of such diabatic states we adopt the criterion underlying the generalized Mulliken–Hush (GMH) model [8, 26, 27, 28], whereby the diabatic states are those which are diagonal with respect to the component of the dipole moment operator along the charge-transfer direction (chosen, for example, as the direction of the adiabatic dipole moment charge associated with a given ET process). Related analysis is given in Refs. [29, 30].

This criterion gives the maximally charge localized states. In many cases, a two-state space suffices (denoted later as the two-state approximation, TSA) for representing the desired D and A states. Rust et al. [28] have recently discussed a quantitative criterion for assessing the adequacy of the TSA relative to an expanded multistate implementation of the GMH model, and related results have been reported [27, 31]. The TSA proves to be sufficient for the cases dealt with in the following discussion, and the key GMH relationships can be compactly expressed as follows:

$$H_{DA}^{d} = \mu_{12}^{a} \Delta E_{12}^{a} / \Delta \mu_{DA}^{d}, \tag{16}$$

$$er_{DA} \equiv \Delta \mu_{DA}^{d} = \left[\left(\Delta \mu_{12}^{a} \right)^2 + 4 \left(\mu_{12}^{a} \right)^2 \right]^{1/2}, \tag{17}$$

where the superscripts d and a are included to emphasize the distinction between the diabatic (d and a) and adiabatic (1 and 2) states quantities in the TSA framework, $\Delta\mu$ corresponds to the dipole moment shift, ΔE_{12}^{a} and μ_{12}^{a} are the adiabatic vertical transition energy and transition dipole moment, and r_{DA} provides a useful definition of effective D/A separation, which does not require ad hoc assumptions based on independent structural data. Equation (17) makes clear that $\Delta\mu_{DA}^{d}$ (and hence r_{DA}) may be considerably larger than the corresponding adiabatic quantity $\Delta\mu_{12}^{a}$, which, for example, may be obtained from Stark spectroscopy [32].

Equations (16) and (17) offer a compact prescription for converting adiabatic state information (obtained, for example, from quantum chemical configuration interaction, CI, calculations or from experimental spectroscopic information) into the diabatic quantities involved in models for k_{ET} (e.g., Eq. 1). Estimates of r_{DA} are required in formulating the distance dependence of k_{ET} due to H_{DA}, λ^{s}, and ΔG^{0}, as noted earlier.

A great advantage of the GMH approach is its applicability to arbitrary system configurations (both with respect to solute and with respect to medium coordinates), thus making it valuable for assessing the sensitivity of H_{DA} to various coordinates of interest (i.e., departures from the Condon approximation). Thus the GMH model is equally applicable to the resonant case, as in thermal ET, where the D and A levels at the transition state are equal and $H_{DA}=\Delta E_{12}^{a}/2$ and the nonresonant case, as in optical ET, where the photon energy compensates the mismatch in D and A energies.

Before proceeding to consider specific quantum models for H_{DA} in molecular systems, we address additional factors bearing on the choice of an appropriate electronic space. This space should be suitably flexible in allowing the states involved in ET to respond via polarizability to influences such as coordinate fluctuations and external fields. The importance of the change in α ($\Delta\alpha$) accompanying the ET process has been emphasized in Refs. [14, 15]. In one approach to sampling a variety of solvation situations [15], a fixed two-state space (e.g., based on vacuum solute states) may be supplemented by polarizability parameters which capture that part of the initial and final state polarizabilities not implicitly included in the two-state electronic model. In the examples considered later, an in situ approach is taken, in which a calculation carried out using a suitable CI basis yields a two-state GMH model specifically adapted to each solute/solvent system.

Aside from the purely electronic issues noted earlier, one must of course bear in mind the larger vibronic context. The Condon factorization entailed in k_{ET} as given in Eq. (1) is often a viable approach, which still permits variations in H_{DA} to be examined, but in some cases the overall vibronic context must be considered [33, 34].

Models for H_{DA}

Pathway models

When the D and A groups in a DBA ET system are relatively weakly coupled to the B, a number of perturbative expressions are available for modeling H_{DA} in the case of resonant D and A levels ($E_{D/A} \equiv E_D = E_A$, as required in thermal ET) [35]. In superexchange B-mediated tunneling a particular sequence of virtual intermediate B states for the tunneling charge defines a "pathway". The familiar nearest-neighbor (NN) pathway of McConnell yields the following picture for a homologous B with n states in a linear sequence [36]:

$$H_{DA} = (T_{DB})(t_{BB'}/\Delta)^{n-1}(T_{BA}/\Delta), \tag{18}$$

where T_{DB} and T_{BA} are the NN "hopping integrals" linking D and A, respectively, to the terminal sites of the B, and $t_{BB'}$ is the hopping integral linking each of the $n-1$ NN pairs of B sites (we assume one B state per site), Δ is the vertical energy gap between $E_{D/A}$ and the energy of the diabatic B states (the so-called tunneling gap or effective tunneling barrier), and in the perturbative limit, T/Δ, $t/\Delta \ll 1$. While a number of other pathways are possible, which when superposed may yield appreciable interference, either constructive or destructive [37, 38, 39, 40, 41, 42], the simple expression in Eq. (18) reveals important qualitative features.[1] The predicted exponential dependence on the number of B units (n) yields an expression for the conventional exponential decay coefficient, β:

$$\beta = -2\ln|t_{BB'}/\Delta|/(\Delta r), \tag{19}$$

where β is defined by

$$|H_{DA}|^2 \propto \exp(-\beta r_{DA}) \tag{20}$$

and r_{DA} is assumed to be a linear function of the mean "length" of each B site, Δr. The β coefficient in Eq. (20) pertains to only one of the factors in Eq. (1) and, as noted previously, should be distinguished from the decay parameter (often also denoted as "β") relevant to the overall rate constant [22].

Equation (18) also reveals that any fluctuation influencing the magnitude of T, t, or Δ may result in non-Condon behavior of H_{DA}. Such an effect may be expected for modes directly affecting orbital overlap (e.g., torsional modes). More subtle effects due to variations in Δ are considered later.

A heterogeneous analog of Eq. (18) is straightforwardly obtained:

$$H_{DA} = (T_{DB1})\left[\prod_{j=1}^{n-1}\left(t_{B_jB_{j+1}}/\Delta_j\right)\right](T_{B_nA}/\Delta_n), \tag{21}$$

[1] The left-hand sides of Eq. (2.55) in Ref. [38] and Eq. (4.16) in Ref. [39] are in error and should be replaced by their reciprocals

where Δ_j is the gap involving the jth B site, and the hopping integrals may be distinct for each NN pair.

Detailed ab initio quantum chemical assessment of Eqs. (18) and (21) using site-localized basis sets reveals that for quantitative purposes, the single NN pathway model may be grossly in error by comparison with exact H_{DA} values calculated independently [37, 40, 41, 42]. Nevertheless, the single pathway form may be very useful in fitting trends in H_{DA} when the T, t, and Δ parameters are defined as suitable effective quantities [41, 43].

An example of two competing pathways, corresponding, respectively, to ET (via intermediate excess-electron B states) and HT (via intermediate ionized B states), is illustrated schematically in Fig. 2. Here, the D, A, and B sites may be taken as components of metal–ligand complexes in bimolecular contact, and the various charge-localized states are distinguished in terms of orbital occupations. As the large gaps between D/A and B (required for the virtual states in the perturbative model) are reduced, the probability of charge injection onto the B (i.e., creating real intermediate states of measurable lifetime) increases, and ultimately a sequential hopping mechanism may become operative.

The possibility of extending the superexchange approach to the nonresonant situation, where $E_D \neq E_A$, as in optical ET, has been discussed in the context of the Mulliken–Hush model [25], leading to a generalized definition of the effective tunneling gap (Δ). The resulting implications for non-Condon behavior have been considered in Refs. [5, 35, 38, 39]. It should be noted, however, that this analysis was limited to a single reaction coordinate.

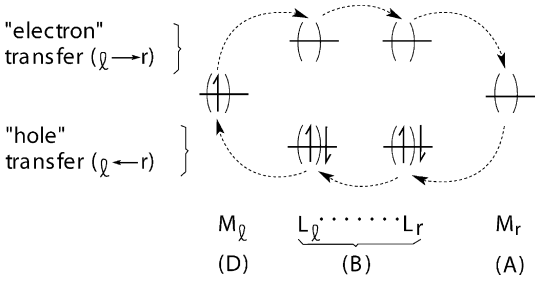

Fig. 2. Schematic representations of thermal bridge-mediated charge transport of the "electron" (*top*, *left* to *right*) and "hole" (*bottom*, *right* to *left*) type, illustrated for the case of intermolecular ET between two metal/ligand (M/L) complexes, where $D \equiv M_l$, $B \equiv L_l...L_r$, and $A \equiv M_r$. The intermediate states for the hole and electronic processes involve, respectively, charge localization based on the filled ("valence") and empty ("conduction") bands of the bridge. When the energy gaps separating the common (resonant) D/A level from those of the bridge (taken here as equal, as in a homologous spacer) is large relative to the magnitude of coupling between D and A groups and the bridge, coherent (superexchange) tunneling occurs between D and A, and the intermediate bridge states are "virtual". As the gaps become smaller, the residence lifetimes of the excess charge on the bridge sites increases, leading eventually to a conventional sequential hopping process from D to A

Quantum chemical evaluation

Evaluation of H_{DA}, for example, using the GMH model, may be carried out on the basis of quantum chemical calculations (self-consistent field, SCF or CI) for the DBA systems, either in a vacuum or in a surrounding polar medium. For large organic aggregates the all-valence semiempirical INDO/s (developed by Zerner et al. [44]) and AM1 models [45] are very useful, and the INDO/s model also gives access to inorganic and organometallic complexes [46, 47]. It is important to validate the performance of the semiempirical methods by comparison with ab initio results. In a number of cases agreement to within 25% has been observed [43, 46]. Generally, reasonable agreement between INDO/s [47] and ab initio [48] results for metallocene/metallocenium H_{DA} values was found, although the comparison here is complicated by the fact that different metal–carbon bond lengths were used in the two sets of calculations.

D/A coupling mediated by organic spacers

Calculated distance dependence

The sensitivity of D/A coupling with respect to details of electronic structure are illustrated here for several families of DBA systems. The selection of systems is motivated in part to facilitate contact with results based on experimental kinetic data, especially that obtained from electrochemical studies involving self-assembled-monolayer film-modified electrodes [49, 50, 51]. The calculated decay coefficient (β) of H_{DA} (Eqs. 19, 20) for several homologous radical cation, $(DBA)^+$, and anion, $(DBA)^-$, systems are presented in Table 1, based on the D, B, and A moieties depicted in Fig. 3. The calculated results were obtained from INDO/s SCF/CI calculations analyzed in terms of the GMH model (Eq. 16) [43, 52]. While ferrocenyl D and A groups are most directly related to some of the systems studied experimentally, it is also of interest to compare the ferrocene (Fc) results with those based on the model D/A CH_2 group [43], which possesses the same carbon hybridization (sp^2) as the cyclopentedienyl (Cp) carbon atoms which link the Fc moieties to the spacers. Indeed, Fc and CH_2 are seen to yield very similar β values, as do also the corresponding radical cation and anion systems.

It should be emphasized that while there is no constraint requiring the quantum calculations to yield exact exponential decay with r_{DA}, in fact for all the homologous systems considered, the numerical results adhered very closely to exponential behavior, consistent with the simple NN model given in Eq. (18).

As expected, a more gradual falloff (smaller β value) is found for conjugated unsaturated spacers relative to the alkane spacers (oligomethylene, OM). More interesting are the variations among the different unsaturated spacers. For planar conformations, incorporation of phenylene (P) groups into the spacer (oligo-*p*-phenylene-thynylene, OPE or oligo-*p*-phenylenevinylene, OPV)

Table 1. Sensitivity ofH_{DA} decay to donor/acceptor (D/A) and bridge (B) type in $(DBA)^{\pm}$ systems.Detailed structures are given in Fig. 3. Oligovinylene (OV), oligo-*p*-phenylenevinylene (OPE), oligo-*p*-phenylenevinylene (OPV), oligomethylene (OM), ferrocene (Fc). Table 1 of Ref. [52], reprinted with kind permission. Copyright 2003, American Chemical Society

D/A	B		β ($Å^{-1}$)		Exp
	Conformation		Calculated		
			Radical cations	Radical anions	
CH_2	OV	Planar	0.31	0.32	≥0.2[a]
CH_2	OPE	Planar	0.39	0.43	0.4[c,d], 0.6[c,e]
		Randomized	0.51	0.54	
Fc[b]	OPE	Planar	0.36	–	
CH_2	OPV	Planar	0.43	0.46	–[g]
	OPV	Planar–CH_3O–subst.[f]	0.46	–	
Fc[b]	OPV	Planar	0.42	–	
CH_2	OM	Staggered	0.83	1.00	0.9 ± 0.1[h]

[a][86, 87,88]; based on Mulliken–Hush [25] analysis of optical data
[b]Hole ground states are localized in the $3d_{x^2-y^2}$ Fe orbitals, where z is the Fc axis and x is the long axis of the bridge
[c]Based on measured rate constants
[d]Ref. [56]
[e]Ref. [55]
[f]The two ortho hydrogens nearest to the D attachment site of the first phenylene group were replaced with methoxy groups
[g]Ref. [51]; $\beta < 0.1$ $Å^{-1}$, based on Arrhenius prefactors
[h]Ref. [50]; based on Arrhenius prefactors for large r_{DA} (> 10 Å); for small r_{DA} (≤ 10 Å),a falloff of distance dependence (i.e., effective β value) is observed [49]

leads to a modest increase in β relative to the polyene reference (oligovinylene, OV). The β values for planar OPE and OPV spacers are quite similar, indicating that the "extra" π bonds in the triple-bonded systems (OPE) are not strongly involved in the superexchange tunneling. It is also seen that methoxy substituents on the OPV spacers (these or other alkoxy substituents are commonly employed in experimental studies [51]) has little effect on β.

Since the intrinsic barrier for rotation about single linker bonds in the OPE spacers is quite small (around k_BT at room temperature), departures from the planar reference framework geometry may be appreciable [8, 43]. Root-mean-square H_{DA} values based on random torsion angles (θ, as in Fig. 3) for the phenylene groups yield a larger β value (around 0.5 $Å^{-1}$), and similar results (6% less) are obtained when the averaging is weighted by Boltzmann factors based on barriers of 0.6 kcal mol^{-1} for each torsional degree of freedom.

Although the tunneling through the unsaturated spacers is dominated by the π-electron manifolds, it is by no means negligible for orthogonal conformations of adjacent moieties [43]; for example, for OPE spacers, the effective hopping integral (t) between adjacent orthogonal PE groups (involving a hyperconjugative mechanism) is about one third of the corresponding value for planar groups. When all the PE groups are twisted 90° with respect to the π plane of coplanar CH_2 D and A groups, thus forcing the tunneling to be mediated by the spacer σ-orbital manifolds, the resulting β value is indeed quite similar (around 1.0 $Å^{-1}$) to that found for the saturated OM spacer.

Hole versus electron tunneling

The GMH analysis yields overall H_{DA} values which implicitly may involve superposition over many superexchange pathways, including the limiting cases of purely ET or HT (Fig. 2). While one might expect charge transfer in radical cation, $(DBA)^+$, and anion, $(DBA)^-$, systems to be strongly dominated, respectively, by hole and electron tunnellng, a detailed analysis reveals a much less clearcut distinction. Table 2 displays estimated gaps for (virtual) hole and electron injection into OPE(1) and OPV (1) spacers in the radical cation systems, based on INDO/s CI calculations including single excitations from the two lowest-energy configurations to configurations of predominantly hole or electron type. These single excitations can be summarized in the following shorthand notation:

$$DBA^+,\ D^+BA \rightarrow DB^+A \text{ (hole transfer)},$$
$$DBA^+,\ D^+BA \rightarrow D^+B^-A^+ \text{(electron transfer)}.$$

The calculated gaps in Table 2 give the energy of the lowest charge-injected B state relative to the resonant initial and final diabatic states (the calculations involved 10–20 CI basis configurations). The gaps are large enough to support the use of perturbative superexchange analysis, even though they are considerably smaller than the corresponding gaps (several electron volts) inferred from analysis of saturated hydrocarbon spacers [37, 38, 39]. The OPE and OPV gaps are comparable (the slightly larger OPV gap correlates qualitatively with the slightly larger β value, Table 1), and we also find that the gap for electron tunneling in the radical cation systems is only 0.1–0.2 eV larger than the hole tunneling gaps.

Alternative hole states

The previous analysis of coupling involving Fc D and A sites was based on ground hole states within the TSA. However, it is well known that the ground hole state of the isolated ferrocenium is degenerate in D_5 point-group symmetry, corresponding to holes of primarily $3d_{x^2-y^2}$ and $3d_{xy}$ character. The fate of this degeneracy when Fc

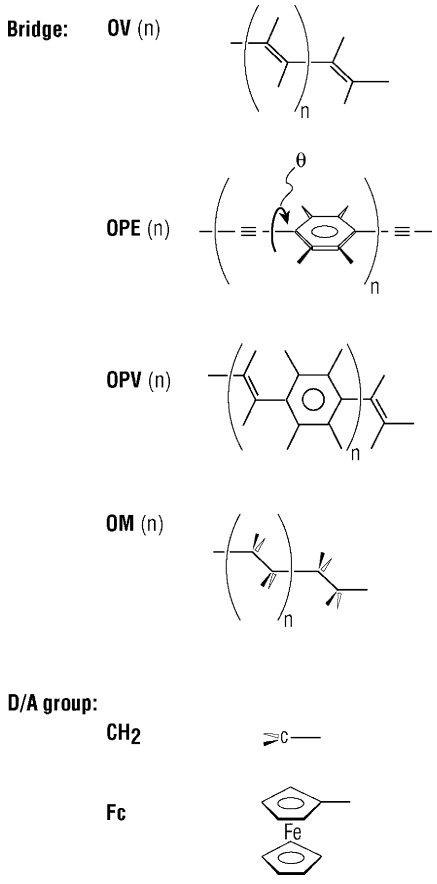

Fig. 3. Molecular components of the DBA systems for which calculations were carried out. Three types of unsaturated bridges were employed: oligovinylene (*OV*), with a vinylene unit (*V*) plus *n* V repeat units ($n = 1,3,5$); oligo-*p*-phenylenethynylenes (*OPE*), with an ethlynylene unit (*E*) plus *n* PE repeat units ($n = 0$–4); oligo-*p*-phenylenevinylene (*OPV*), with a vinylene unit (*V*) plus *n* PV repeat units ($n = 0$–4). The saturated oligomethylene (*OM*) bridges (in fully staggered conformation) are based on a $(CH_2)_2$ unit plus *n* additional $(CH_2)_2$ repeat units ($n = 1$–4, the number of repeat units given in the caption for Fig. 2 in Ref. [52] is in error by a factor of 2). To keep the notation uncluttered, the CH bonds in the cyclopentadiene (*Cp*) rings of the ferrocenyl (*Fc*) D/A groups have been omitted

Table 2. Calculated energy gaps for injecting holes or electrons onto OPE(1) and OPV(1) bridges (respectively, $D^+BA \rightarrow DB^+A$ or $D^+BA \rightarrow D^+B^-A^+$)

D/A	B	ΔE (eV)[a]	
		Hole	Electron
Fc	OPE(1)	1.6	1.8
Fc	OPV(1)	1.6	1.7

[a]Estimates based on restricted single excitation configuration interaction calculations (see text)

hole states are incorporated into spacer-linked DBA systems can have significant consequences for the D/A coupling strength (H_{DA}) [46, 47, 52, 53]. To broaden the perspective here, we also consider a variant of Fc in which the CpFe moiety is replaced by the cyclobutadiene–Co moiety (denoted as CbCo), a replacement which is isoelectronic as far as the metal atom and ligand π electrons are concerned. This complex (Fig. 4), abbreviated as CbCoCp, has been considered by Harrison et al. [54] for its potential role in the design of square-planar conductive arrays.

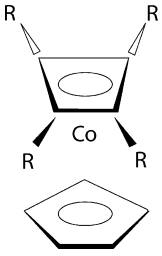

Fig. 4. Cyclobutadiene (*Cb*)/Cp Co sandwich complex (isoelectronic with Fc as far as relevant valence molecular orbitals are concerned). The cases $R = H$ and $R = \varphi$ are considered in Sect. 5 and Tables 3 and 4

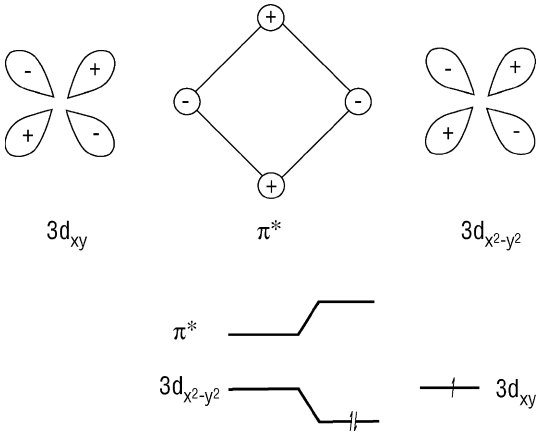

Fig. 5. Splitting of the Co $3d_{x^2-y^2}/3d_{xy}$ degeneracy in CbCoCp due to mixing with the π^* orbital of Cb

In contrast to Fc, the $3d_{x^2-y^2}/3d_{xy}$ degeneracy is broken in the isolated CbCoCp complex (and its tetraphenyl-substituted derivative, (Cbφ_4CoCp, denoted as Cb′CoCp). As indicated schematically in Fig. 5, this splitting can be understood in terms of the local C_{4v} symmetry of the CbCo moiety: in this symmetry, the only interactions between the Cb π orbitals and the Co $3d_{x^2-y^2}$ and $3d_{xy}$ orbitals involve the antibonding orbital of Cb (π^*), which pushes the $3d_{x^2-y^2}$ orbital (b_2 representation in C_{4v}) below the $3d_{xy}$ orbital (b_1 representation) [46, 47, 52]. The significance for electron (or hole) tunneling is clear, since the resulting hole state ($3d_{xy}$-like) cannot delocalize effectively onto the Cb carbon atoms, which are the sites of attachment in extended CbCoCp arrays. Some energy splittings for the mononuclear complexes are displayed in Table 3. These splittings, and those for the local hole states in the binuclear systems in Table 4, are based on restricted-open-shell INDO/s SCF calculations. While φ-substitution (Cb $\rightarrow$ Cb′) reduces the splitting by nearly a factor of 2,

it remains significant relative to k_BT at room temperature, indicating a small thermal population of the state expected to yield the strongest B-mediated D/A coupling. Access could perhaps be achieved via photoexcitation.

Examples of the magnitude of H_{DA} for $3d_{x^2-y^2}$ and $3d_{xy}$ hole states are shown in Table 4, along with the state splittings. For the Fc cases, linkage to the B [OPE(1) or OPV(1), as defined in Fig. 3] yields a splitting of around $2k_BT$ at room temperature, with the strongly coupled $3d_{x^2-y^2}$ hole state as the ground state.

Table 3. Splitting of $3d_{x^2-y^2}$ and $3d_{xy}$ hole states for Fc and $(C_4R_4)Co(C_5H_5)$ (structure given in Fig. 4)

	Hole state[a]	Relative energy (eV)[b]	Point group
Fc	$3d_{x^2-y^2}$, $3d_{xy}$	0.00	D_5
	$3d_{z^2}$	0.48	
$(C_4H_4)Co(C_5H_5)$[c]	$3d_{xy}$	0.00	C_s (C_{4v})[d]
	$3d_{z^2}$	0.27	
	$3d_{x^2-y^2}$	0.33	
$(C_4\varphi_4)Co(C_5H_5)$[e]	$3d_{xy}$	0.00	C_1 (C_4)[f]
	$3d_{x^2-y^2}$	0.18	

[a]The 3*d*-type hole states are based on a coordinate system where the *z*-axis is perpendicular to the ring planes and where, for $(C_4R_4)Co(C_5H_5)$, the *x*- and *y*-axes are parallel to the diagonals of the C_4 ring. Thus the C_4 carbons lie in the nodal planes of the $3d_{xy}$ orbital (Fig. 5)
[b]The ground state and low-lying excited states were obtained from separate direct self-consistent-field calculations
[c]Fig. 4(R = H)
[d]Local point group symmetry of the cyclobutadiene (*Cb*)Co moiety
[e]Fig. 4($R = \varphi$); the four φ substituents were arranged in a propeller-like configuration with respect to the Cb ring, with Cb/φ diherdral angles taken as 35° [54]
[f]Local point group symmetry of Cb′Co moiety

Table 4. Quasi-degenerate hole states at tethered Fc and Cb′Co–cyclopentadiene (*Cp*) D and A sites

	3*d*-hole type[a]	H_{DA} (cm^{-1})[b]	Relative energy (eV)[b]
$[Fc\ OPE(1)Fc]^+$	$3d_{x^2-y^2}$	177	0.000
	$3d_{xy}$	2	0.058
$[FcOPV(1)Fc]^+$	$3d_{x^2-y^2}$	140	0.000
	$3d_{xy}$	0.4	0.051
[(Cb′CoCp)]-	$3d_{xy}$	3.1	0.000
$[(Cb'CoCp)]^+$[c]	$3d_{x^2-y^2}$	111	0.170

[a]Dominant character of the calculated hole state, where *z* is the long axis of the Fc and Cb′CoCp units, and the *x*-axis is aligned with the single bonds linking the D/A rings to the bridge. In the $3d_{xy}$ hole states, the hole resides predominantly in an Fe (or Co) orbital which mixes with the Cp (or Cb′) molecular orbital bearing a node on the carbon atom linked to the bridge (Fig. 5), thus accounting for the very small H_{DA} magnitudes
[b]Based onself-consistent-field/configuration interaction calculations and generalized Mulliken–Hush analysis, as described in the text
[c]The monomers are covalently linked by a biphenylene bridge formed from adjacent phenyl substituents (one from eachCb′ moiety) and assigned a dihedral angle of 35° (see also footnote e of Table 3)

For the biphenylene-linked CbCoCp units (formed by the para linking of a φ substituent from each Cb′CoCp monomer), the splitting remains about the same as for the isolated Cb′CoCp, leaving the weakly coupled system ($3d_{xy}$ type) as the ground state.

The examples given here offer important caveats concerning the use of the TSA in cases of quasi-degenerate systems (other examples arising either from spatial or from spin effects have been noted in Refs. [46, 47, 53]). Of particular note is the great variability in coupling strength associated with the distinct nodal structure of the different members of a quasi-degenerate set, a fact which may be exploited for control of tunneling.

Comparison of calculated H_{DA} distance dependence with experiment

It was emphasized earlier that the distance dependence of H_{DA}, represented by the calculated β coefficients (Eqs. 19, 20) in Table 1, is not necessarily the same as the "β" obtained from the distance dependence of the overall k_{ET} values. Within the weak-coupling (nonadiabatic) limit, as in Eq. (1), these differences may arise from the distance dependence of $\Delta G^{\dagger}$ (Eq. 2) for relatively short D/A separations ($r_{DA} < 10$–15 Å). At very short separations (typically, $r_{DA} \leq 5$ Å) the nonadiabatic framework, which underlies Eqs. (19) and (20), may be inappropriate owing to strong D/A coupling.

For most of the cases represented in Table 1, experimental data permit an estimation of β for H_{DA}, either from Mulliken–Hush analysis [25] of optical data or Arrhenius analysis of thermal kinetic data [49, 50, 51]. The β results for the OV systems (0.2 $Å^{-1}$ and greater) are consistent with the calculated value and support a nonadiabatic mechanism. This is also true for the OM systems in the longer range of r_{DA} values (10 Å and greater) [49, 50, 51].

Electrochemical kinetic data for OPE systems including 2–6 PE units, with either unsubstituted [55] or alkoxy-substituted [56] phenylene moieties, yield β values (based on overall k_{ET}) spanning a range (0.4–0.6 $Å^{-1}$) which includes the calculated values for planar (0.39 $Å^{-1}$) and randomized (0.51 $Å^{-1}$) spacer conformations [43, 46, 47]. However, more recent [57] kinetic measurements suggest that the r_{DA} dependence of k_{ET} for the OPE systems may not be fully monotonic, and further mechanistic analysis seems to require a more detailed understanding of the conformational distributions pertaining to the systems studied experimentally, including the likely significant role of intermolecular interactions in controlling the torsional angles within a given OPE (see also Ref. [58]).

Turning now to the OPV systems, we note that the experimental Arrhenius prefactors decay only weakly out to around $r_{DA} = 30$ Å (the nominal β value is 0.1 $Å^{-1}$ or less), thus suggesting a dynamical bottleneck for the ET process outside of the TST framework (e.g., some diffusional mode involved in the redox process) [51]. For these thermal ground-state processes, thermo-

dynamic data suggest tunneling gaps (Δ, as in Eq. 18) large enough (around 1 eV and greater) to preclude a sequential hopping mechanism, although such a mechanism has been invoked for photoinitiated ET kinetics involving OPVs in which much smaller gaps (less than 0.1 eV) were estimated in some of the longer members ($n = 3$–5) of the homologous series [59].

Finally, some further comments about the saturated spacers (OM) are warranted. Even though a nonadiabatic mechanism for the longer oligomers is not in doubt, with good agreement between calculated and experimental estimates of β (around 1.0Å^{-1}), the experimental data indicate a falloff from linearity of the logarithm of the Arrhenius prefactor for $r_{DA} \lessapprox 10$ Å. For electronically saturated spacers, this is a surprising result, once again suggesting that factors outside the simple nonadiabatic TST framework may be controlling the experimentally observed ET processes, including possibly alteration of the self-assembled-monolayer film structure [49].

In the foregoing, we have seen that calculated D/A coupling and its distance dependence are consistent with experimental charge-transfer data in a number of instances. Nevertheless, other dynamical factors may be crucial in determining overall kinetic mechanisms in some cases.

Solvent contributions to non-Condon effects

The primary influence of solvent on ET kinetics is its contribution to the activation free energy (e.g., as given by the classical expression in Eq. 2) through fluctuations in the low-frequency polarization modes of the medium. These modes may also influence the electronic coupling (i.e., H_{DA}). The nature of such solvent-driven non-Condon behavior has been discussed in the literature [4, 5, 6, 14, 15, 60, 61, 62], and we examine this topic in the remainder of the present study. In addition to the CS ET process introduced in Sect. 2 (Fig. 1), involving overall neutral systems (DBA and D^+BA^-), we will also consider the complementary charge shift (CSh) process, $DBA^+ \rightarrow D^+BA$. Even if corresponding DBA and DBA^+ systems are isoelectronic, the respective ET energetics may be quite distinct, for example, the absence of a D/A Coulombic term in the driving force ($-\Delta G^0$) for the CSh process [23].

Optical ET: absorption versus emission for CSh in a polar medium

Matyushov and coworkers [14, 15] have emphasized that inertial (low-frequency) modes may lead to pronounced non-Condon ET behavior in polar solvents. As an example of such an effect we consider optical CSh for a DBA^+ system in which the A^+ moiety, an acridinium cation, is linked by a *p*-phenylene spacer to an aniline D group (Fig. 6). This molecular species is abbreviated as ABPAC [9-(aminobiphenyl)-10-methylacridinium]. Charge transfer in this and related systems in polar solvents has been studied by Jonker et al. [63] and Jones and coworkers [64]. A full account of the ET energetics is of course a major computational task, including the need to consider the dependence of properties on torsion angles (especially the θ angles indicated in Fig. 6). Preliminary results for the gas-phase system using ab initio and INDO/s calculations have been reported by Rust et al. [28], and additional calculations are underway [65]. Our current objective is simply to present some sample results based on a model which allows a comparison of the influence of solvent polarity on vertical absorption and emission:

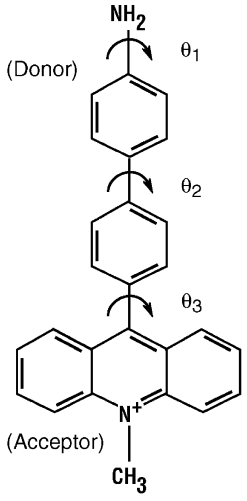

ABPAC
(Amino-BiPhenylene-ACridinium)

Fig. 6. Structure of 9-(aminobiphenyl)-10-methylacridinium (*ABPAC*) and definition of torsion angles θ_1–θ_3. As drawn, all $\theta = 0°$

$$DBA^+ \xrightarrow{h\nu} D^+BA \text{ (absorption)},$$

$$D^+BA \xrightarrow{-h\nu} DBA^+ \text{ (emission)},$$

where $DBA^+ \equiv$ ABPAC. For this purpose we have maintained a fixed ABPAC molecular structure (the estimated ground + state structure determined from AM1 [45] and universal force field (UFF [66]) calculations)[1]. The electronic structure calculations are based on an extended AM1 Hamiltonian including a nonequilibrium continuum reaction field term H_{RF}^{ne} so that in each case (absorption or emission) the fast solvent modes (the optical response controlled by ϵ_∞) are in equilibrium with the final state in the vertical process, whereas the slow modes (the inertial response governed by the effective inertial dielectric susceptibility, proportional to $\epsilon_0 - \epsilon_\infty$) are in equilibrium with the initial state. The reaction field employed here [67] differs from the commonly used polarized continuum models [68] in that it incorporates

[1]UFF coordinates for ABPAC were determined by J. Lappe and R.J. Cave (private communication)

Table 5. Calculated solvent contribution to vertical absorption and emission in 9-(aminobiphenyl)-10-methylacridinium. Results based on vertical charge transfer, using estimated ground-state geometry ($\theta_1 = 0°$, $\theta_2 = 40°$, $\theta_3 = 85°$; see Fig. 6 and text)

$\epsilon_0/\epsilon_\infty$[a]	Absorption			Emission		
	ΔE_{12} (eV)	$\Delta\mu_{12}$ (D)	H_{DA} (10^2 cm^{-1})[b]	ΔE_{12} (eV)	$\Delta\mu_{12}$ (D)	H_{DA} (10^2 cm^{-1})[b]
1.0/1.0	2.8	31.8	5.4	2.8	31.8	5.4
1.8/1.8	2.6	39.3	3.7	2.6	39.3	3.7
7.0/1.8	2.8	37.8	4.2	1.9	41.7	2.8
37.5/1.8	3.0	36.8	4.9	1.7	42.3	2.7

[a]Static and optical dielectric constants used in the reaction field calculations; the radial increment δ [69] was assigned the mean value 1.8 Å in all the reaction field calculations
[b]H_{DA} estimates based on generalized Mulliken–Hush analysis in the framework of the two-state approximation (Eq. 16)

distinct effective cavities for optical and inertial response (the "frequency-resolved cavity model" [69]), and it is formulated for the limiting case of fast solvent electronic response time relative to that of the transferring charge of the solute. This latter approach (quite similar to the BO model of Kim and Hynes [70]) seems reasonable for the present case, where the energy gap associated with the ET process is considerably smaller than the charge-transfer gaps controlling the solvent polarizability. It also has the advantage of yielding initial and final states which are orthogonal (for a fixed inertial polarization of the solvent, as in a vertical process). Since we are only interested in the solvent effect, the possibility of conformational relaxation (e.g., via the θ angles indicated in Fig. 6) in the emitting state is not considered here. The fixed θ values used in the calculations (ground-state estimates) are 0° (θ_1), 40° (θ_2), and 85° (θ_3). X-ray crystal structure data for various aryl–acridinium species yields θ_3 values in the range around $70 \pm 10°$ [71]. The results reported in Table 5 and discussed later are based on AM1/CI including the ground SCF configuration and around 40 CI basis states obtained as single excitations from the ground configuration.

The data in Table 5 probe the influence of the inertial solvent response with respect to two "degrees of freedom": the columns reflect variation in ϵ_0 (for ϵ_∞ fixed at 1.8, a typical value for organic solvents), and each row (for a given ϵ_0) samples two points along the solvent reaction coordinate (the minimum free-energy points for the initial and final states). The three ϵ_0 values selected correspond to a nondipolar ($\epsilon_0 = \epsilon_\infty = 1.8$), a weakly dipolar ($\epsilon_0 = 7$, similar to the value for tetrahydrofuran), and a strongly polar ($\epsilon_0 = 37.5$, representing acetonitrile) solvent. For each transition the calculated vertical energy gap (ΔE) and dipole moment shift ($\Delta\mu$) are given, as well as the H_{DA} value inferred from GMH analysis within the TSA (found to be quite adequate according to the criterion of Ref. [28]). These quantities were introduced in connection with Eq. (16). The qualitative trends in ΔE are in accord with the simple diabatic Marcus expression, based on the assumption of linear solute/medium coupling [4, 11],

$$\Delta E_{abs,em} = \lambda \pm \Delta G^0, \tag{22}$$

provided the dominant solvent dependence is due to λ. The solvent dependence of ΔG^0 is expected to be smaller, depending on the difference in access of the solvent to the hole when it resides on the D and A sites. The present calculations suggest that the final state (i.e., hole on the aniline site) is more strongly solvated than the initial state (acridinium hole site); i.e., ΔG^0 for the CSh process becomes less positive with increasing ϵ_0.

While Eq. (22) offers a useful guideline for expected trends, we note that the current calculations, which yield (implicitly) distinct intial and final state polarizabilities ($\Delta\alpha \neq 0$), are not subject to the limitation of global linearity underlying Eq. (22). The consequences of $\Delta\alpha \neq 0$ are discussed in Refs. [14, 15].

The results for H_{DA} reveal appreciable non-Condon behavior. For a given $\epsilon_0 \neq \epsilon_\infty$, H_{DA} decreases as η changes from the value for vertical absorption to that for the emission (i.e., corresponding to equilibrium, respectively, with the ground and CSh states). Of course for $\epsilon_0 = \epsilon_\infty$, there is no inertial response (in the present dipolar dielectric model), and thus the listed quantities are the same for absorption and emission. The monotonic trend of H_{DA} as ϵ_0 increases (for fixed ϵ_∞) is opposite for the absorption (increasing) and emission (decreasing) processes, but is well correlated with the associated dipole shifts ($\Delta\mu$). The larger $\Delta\mu$ values indicate tighter localization of the D and A states (the dominant effect is found to be at the D-site), and it is plausible that this would tend to reduce the magnitude of the corresponding coupling element. As a result of this variation of H_{DA} with inertial solvent polarization, the precise H_{DA} value for a given ET process will depend on the location along the reaction coordinate (η) pertinent to that particular process. This non-Condon influence of the inertial solvent modes is likely to be enhanced by the state-dependent polarizability implicit in the CI wavefunctions employed in the calculations. Effects of this type have been considered in Ref. [60].

Non-Condon effects in superexchange tunneling

The important role of the tunneling gap, Δ, was noted earlier (see Eqs. 18, 19). Obviously any fluctuation in Δ can provide a contribution to non-Condon behavior of

H_{DA}. While this potential role of thermal fluctuations has long been appreciated, their energy scale (1 eV and lower) may render such effects minor if the basic electronic gaps (Δ) are several electron volts in magnitude, as expected for many DBA systems [4, 5, 6, 35, 72, 73], especially those involving saturated organic spacers [37]. However, when the gaps themselves become of the order of 1 eV (hole transport in DNA duplexes is a recent example of potential interest [74]), the role of fluctuations must be carefully evaluated. These effects have been considered for various special cases in the literature, including a model by Marcus and Sutin [4] using two harmonic oscillator modes (see also the more general analysis and the molecular dynamics results reported in Ref. [73]). Here we present a general model, within the framework of the original classical linear response model of Marcus [11]. The main focus is on the effect due to inertial solvent response, where additive partitioning of energy quantities into site contributions is not generally possible [75], but for completeness, molecular contributions (''inner shell'') are also included.

In particular, we wish to formulate Δ as a function of progress along the ET reaction coordinate, η (Eq 9), with primary interest in the gap at the transition state for thermal ET (where $\eta = \eta^{\dagger} = 0$). Note that η refers to the overall ET process and is distinct from the reaction coordinate associated with the injection process (e.g., for overall CS of the type $DBA \rightarrow D^{+}BA^{-}$, the hole injection corresponds to $DBA \rightarrow DB^{+}A^{-}$). The current approach may be contrasted with simpler models in which the energetics of all states are restricted to profiles along a single common reaction coordinate [5, 6, 35, 72] (for a general discussion of multiple reaction coordinates see Ref. [76]). Furthermore, the gaps considered here differ from the effective gaps defined [5, 35] in conjunction with the Mulliken–Hush model [25].

In the case of quantized molecular modes, the classical approach employed here would require modification. For example, the analysis could be applied to the vibronically-resolved expression given in Eq. (13), in which each vibronic component is governed by a common classical solvent reaction coordinate (Eq. 14b), but with distinct expressions for effective coupling (Eq. 14a) and driving force (Eq. 14c) for each v,w pair.

The expressions presented later are all based on the following representation of a nonequilibrium solvation free energy in the linear response framework [11]:

$$G_{\mathrm{non-eq}}(\rho, \rho') = G_{\mathrm{eq}}(\rho) + \lambda(\Delta\rho), \tag{23}$$

where $\Delta\rho = \rho' - \rho$, and the fast (optical) and slow (inertial) modes of the solvent are in equilibrium, respectively, with solute charge densities ρ and ρ' For vertical absorption or emission from solvent-equilibrated states, the initial solute state determines $\rho = \rho'$; after the transition, ρ becomes the final solute state charge density, and ρ' remains fixed.

For a homogeneous solvent medium the classical solvent reorganization energy may be represented as

$$\lambda^{S} = (1/8\pi)\int_{V_s} \mathrm{d}V\left(\left|\overline{D}(\Delta\rho, \varepsilon_\infty)\right|^2/\varepsilon_\infty - \left|\overline{D}(\Delta\rho, \varepsilon_0)\right|^2/\varepsilon_0\right), \tag{24}$$

where $\mathbf{D}$ is the electric displacement field and V_s is the volume containing the solvent, and where spatial locality has been assumed. Equation (24) represents the general case in which $\mathbf{D}$ is a function of the dielectric constant, in contrast to the common approximation implicit in Eq. (5), in which such ''image effects''are neglected [77].

We now adopt the notation λ^{s}_{XY}, where X and Y are the sites on which the transferring charge is predominantly localized in a given ET step (represented by the density shift $\Delta\rho$). Thus λ^{s}_{DA} refers to the overall ET process. Consideration of B-mediated tunneling later will entail additional λ^{s} quantities (λ^{s}_{AB}, λ^{s}_{DB}, etc). For the simple case of a point charge transferring between the centers of spherical D and A sites, the familiar two-sphere approximation of Marcus is given by [11]

$$\lambda^{s}_{DA} = (\Delta q)^2(1/\varepsilon_\infty - 1/\varepsilon_0)(1/2r_D + 1/2r_A - 1/r_{DA}), \tag{25}$$

where Δq is the magnitude of the shift in the point charge at each site in the ET process. Molecular (''inner sphere'') λs, taken as additive with respect to D, B, and A sites, will be denoted λ^{in}_{D}, etc (cf., the discussion following Eq. 3). For convenience we use the dimensionless reaction coordinate m for the overall ET process, related to η (Eq. 9) by the following linear transformation

$$m = \left(\lambda_{DA} + \Delta G^{0}_{DA} - \eta\right)/2\lambda_{DA}, \tag{26}$$

where the initial and final diabatic minima correspond to $m = 0$ and $m = 1$, and where $\lambda_{DA} = \lambda^{s}_{DA} + \lambda^{in}_{D} + \lambda^{in}_{A}$. If ρ_i and ρ_f are the initial and final state solute charge densities in the ET process, then for an arbitrary fluctuation along the reaction coordinate, the corresponding ρ' in Eq. (23) may be represented as

$$\rho' = \rho_i + m(\rho_f - \rho_i). \tag{27}$$

Exploiting Eqs. (23) and (27) yields very compact expressions for $\Delta^{v}(m)$, where the superscript v is added to emphasize the vertical nature of the tunneling gap. The following expression applies to either CS or CSh processes, and has been adapted to the HT case:

$$\begin{aligned}\Delta^{v}(m) = {} & \left(\Delta G^{0}_{AB} + \lambda^{s}_{AB} + \lambda^{in}_{A} + \lambda^{in}_{B}\right) \\ & (>0) \\ & -m\left(\lambda^{s}_{DA} + \lambda^{s}_{AB} - \lambda^{s}_{DB} + 2\lambda^{in}_{A}\right) \\ & (<0),\end{aligned} \tag{28}$$

where the net negative sign of the contribution linear in m is indicated.We summarize here the subscript notation used for the various steps involved in the CS and CSh hole-tunneling processes:

CS/h:				CSh/h:			
DA:	DBA	$\rightarrow$	D^+BA^-	DA:	DBA^+	$\rightarrow$	D^+BA
AB:	DBA	$\rightarrow$	D^+BA^-	AB:	DBA^+	$\rightarrow$	DBA
DB:	DB^+A^-	$\rightarrow$	D^+BA^-	DB:	DB^+A	$\rightarrow$	D^+BA
A:	A	$\rightarrow$	A^-	A:	A^+	$\rightarrow$	A
B:	B	$\rightarrow$	B^+	B:	B	$\rightarrow$	B^+

For the analogous ET process (not considered here), one simply makes the straightforward changes in the definition of the AB, DB, and B subscript notation [corresponding for CS, respectively, to $DBA \rightarrow D^+B^-A$, $D^+B^-A \rightarrow D^+BA^-$, and $B \rightarrow B^-$, and with A replaced by D ($D \rightarrow D^+$), and with analogous changes made for the CSh case], maintaining the compact additive form of Eq. (28).

Equation (28) makes clear that relative to the vertical gap at the initial state equilibrium ($m=0$), progress along the reaction coordinate toward the transition state decreases the gap (within the "normal" Marcus regime [4]), since the coefficient of $-m$ is positive (this is not analytically true, but is the case for realistic estimates of the λ^s terms). In terms of the superexchange model (see Eqs. 18, 19, 20) such a decrease in gap will tend to enhance the tunneling and decrease its decay rate (β). When the reference gap $\Delta^v(0)$ is relatively small in magnitude (i.e., around 1 eV), the enhancement due to thermal activation may be appreciable. Note that at the ET transition state, $m^\dagger = \left(\lambda_{DA} + \Delta G^0_{DA}\right)/2\lambda_{DA}$ [11].

Tong et al. [78] have noted that from the point of view of quantum chemistry, where calculated energies for species in vacuo are readily available, it is convenient to define $\Delta^v(m)$ relative to the corresponding vertical vacuum gap (denoted here as Δ^{vv}). Expressions very similar to that in Eq. (28) are obtained, but here some distinctions between CS and CSh processes must be made:

$$\Delta^v_{CS/h}(m) = \underset{(>0)}{\Delta^{vv}_{CS/h}} + \underset{(<0)}{\left(\Delta G^0_{AB}\right)^\infty} - m\underset{(<0),}{\left(\lambda^s_{DA} + \lambda^s_{AB} - \lambda^s_{DB} + 2\lambda^{in}_A\right)} \tag{29}$$

$$\Delta^v_{CSh/h}(m) = \underset{(>0)}{\Delta^{vv}_{CSh/h}} + \underset{(\sim 0)}{\left(\Delta G^0_{AB}\right)^\infty} + \underset{(>0)}{\left(\lambda^s_{AB} + \lambda^s_A - \lambda^s_B\right)} - m\underset{(<0),}{\left(\lambda^s_{DA} + \lambda^s_{AB} - \lambda^s_{DB} + 2\lambda^{in}_A\right)} \tag{30}$$

where $\left(G^0_{AB}\right)^\infty$ is the contribution to ΔG^0_{AB} due to optical (electronic) solvation, and where the terms linear in m are the same as in Eq (28).In Eq. (30) the quantity $\lambda^s_A - \lambda^s_B$ is equivalent to the inertial contribution to ΔG^0_{AB}. Like Eq. (28), Eqs. (29) and (30) pertain to HT, but once again, adaptation to the electron tunneling case is straightforward. For hole tunneling in CS, $\Delta^v(m)$ is expected to be smaller than the Δ^{vv} reference, whereas for CSh, a tradeoff between positive and negative terms is revealed. In the special limiting case when all λ^s_{XY} are assumed to be additive with respect to site contributions ($\lambda^s_{XY} = \lambda^s_X + \lambda^s_Y$; XY = D, B, or A) and also with all λ_X equal so that $\lambda_{DA} = 2\lambda_A$, and with neglect of $\left(G^0_{AB}\right)^\infty$, Eq. (30) becomes (for $m = m^\dagger = 1/2$, the transition state value for thermoneutral ET)

$$\Delta^v_{CSh/h}(1/2) \;=\; \Delta^{vv}_{CS/h} + \lambda_{DA}/2 - \lambda^{in}_{DA}/2, \tag{31}$$

where, subject to the stated assumptions, all λ terms are expressed in terms of λ_{DA}.Thus the gap is increased by the reorganization energy to the extent that λ^s_{DA} exceeds λ^{in}_{DA} (note that $\Delta^{vv}_{CS/h}$ includes a positive contribution due to λ^{in}_{AB} equal under the simplifying assumptions adopted here to λ^{in}_{DA}. An expression similar to Eq. (31) was employed in Ref. [78].The foregoing results underscore the importance of obtaining accurate estimates of solvent reorganization energies. Recent efforts to evaluate λ^s for HT in DNA systems on the basis of continuum-level formulations have revealed the great sensitivity of λ^s magnitude to details of the dielectric model [78, 79]. Equations (28), (29), and (30) are general, requiring only that the states of the transferring charge can be expressed in terms of the appropriate diabatic charge densities (ρ_D, ρ_A, or ρ_B, where B is a particular site of the spacer), and assuming linear coupling of solute and solvent. In practice, the simple two-sphere model (Eq. 25) may provide useful estimates of λ^s, if suitable values of the dielectric constants and effective radii are available. In complex inhomogeneous media (as, for example, in the case of DNA [80, 81]), generalized continuum models are available, but sensitivity to specification of dielectric parameters remains an important issue [79].To complement the analysis we note that considerable perspective on the role of nuclear motion in D/A coupling (including both solute and solvent modes) has been provided by molecular level treatments [12, 61, 82, 83, 84, 85] combining electronic structure calculations with molecular dynamics simulations and surface-hopping trajectory techniques [85].

Summary

In this overview we have treated long-range electronic coupling of local D and A sites (H_{DA}) in the context of thermal and optical ET, with special focus on formulations amenable to practical computational implementation. The importance of choosing a suitably flexible electronic state space for such computations has been emphasized, and the sensitivity of H_{DA} magnitudes with respect to different types of nuclear coordinates (D/A separation, r_{DA}), torsion angles, and ET reaction coordinates (including both discrete molecular and solvent inertial contributions) has been considered in detail. The

distance dependence of H_{DA} (represented by the mean exponential decay coefficient β) has been evaluated for homologous intramolecular DBA radical ion systems, in which Fc or methylene D and A groups are linked by a variety of organic spacers, both saturated and unsaturated. These results have been shown to be in generally good agreement with estimates based on experimental kinetic and optical ET studies. Such comparisons are complicated in some cases, however, owing to uncertainty about torsion angles and overall kinetic mechanisms in the systems studied experimentally.

The response of the magnitude of H_{DA} to variations in inertial medium polarization (i.e., non-Condon behavior) has been investigated. Limited CI calculations based on a nonequilibrium reaction field Hamiltonian in the case of intramolecular ET between acridinium and aniline-based D and A sites indicate appreciable sensitivity to location along the solvent reaction coordinate (inferred by comparison of coupling for vertical absorption and emission) and to solvent polarity. This sensitivity may be enhanced by the state-dependent polarizability of the solute, as represented by the CI wavefunctions employed in the calculations.

In the case of superexchange tunneling, the sensitivity of the tunneling gap (Δ) to progress along the reaction coordinate (including molecular as well as solvent contributions) has been formulated in terms of a general linear response framework. When the gap is relatively small (i.e., of the order of the magnitude of reorganization energies), the corresponding sensitivity of H_{DA} (e.g., via Eq. 18) may be significant.

Acknowledgements The author is grateful to R.J. Cave and M. Rust for making available molecular coordinates for acridinium derivatives, and to R.J. Cave for several valuable discussions. This work was supported by the Division of Chemical Sciences, US Department of Energy, under grant DE-AC02-98CH10886.

References

1. Balzani V (ed) (2001) Electron transfer in chemistry, vols I–V. Wiley-VCH, Weinheim
2. (a) Jortner J, Bixon M (eds) (1999) Adv Chem Phys 106; (b) Jortner J, Bixon M (eds) (1999) Adv Chem Phys107
3. Jortner J, Ratner M (eds) (1997) Molecular electronics. Blackwell, Oxford
4. Marcus RA, Sutin N (1985) Biochim Biophys Acta 811:265
5. Sutin N (1991) Adv Chem Ser 228:25
6. Newton MD, Sutin N (1984) Annu Rev Phys Chem 35:437
7. Jortner J, Bixon M (1999) Adv Chem Phys 106:35
8. Newton MD (2001) In: Piotrowiak P (ed) Principles and theories, vol I, part 1. Wiley-VCH, Weinheim, pp 3–63
9. Skourtis SS, Beratan DN (2001) In: Piotrowiak P (ed) Principles and theories, vol I, part 1. Wiley-VCH, Weinheim, pp 109–125
10. (a) Gould IR, Noukakis D, Gomez-Jahn L, Young RH, Goodman JL, Farid S (1993) Chem Phys 176:439; (b) Marcus RA (1989) J Phys Chem 93:3078
11. Marcus RA (1956) J Chem Phys 24:966
12. Ungar LW, Newton MD, Voth GA (1999) J Phys Chem B 103:7367
13. Calef DF, Wolynes PG (1983) J Phys Chem 87:3387
14. (a) Matyushov DV, Voth GA (2000) J Chem Phys 113:5413; (b) Matyushov DV, Voth GA (1999) J Phys Chem A 103:10981; (c) Small DW, Matyushov DV, Voth GA (2003) J Am Chem Soc 125:7470
15. Matyushov DV, Newton MD (2001) J Phys Chem A 105:8516
16. Schenter GK, Garrett BC, Truhlar DG (2001) J Phys Chem B 105:9672
17. Tachiya M (1989) J Phys Chem 93:7050
18. Sutin N (1983) Prog Inorg Chem 30:441
19. Jortner J, Bixon M (1988) J Chem Phys 88:167
20. (a) Onuchic JN, Beratan DN, Hopfield JJ (1986) J Phys Chem 90:3707; (b) Medvedev ES, Stuchebrukhov AA (1997) J Chem Phys 107:3821
21. Brunschwig BS, Logan J, Newton MD, Sutin N (1980) J Am Chem Soc 102:5798
22. Yonemoto EH, Saupe GB, Schmehl RH, Hubig SM, Riley RL, Iverson BL, Mallouk TE (1994) J Am Chem Soc 116:4786
23. Davis WB, Hess S, Naydenova I, Haselsberger R, Ogrodnik A, Newton MD, Michel-Beyerle M-E (2002) J Am Chem Soc 124:2422
24. Jortner J, Bixon M, Langenbacher T, Michel-Beyerle ME (1998) Proc Natl Acad Sci USA 95:12759
25. Hush NS (1968) Electrochim Acta 13:1005
26. Cave RJ, Newton MD (1996) Chem Phys Lett 249:15
27. Cave RJ, Newton MD (1997) J Chem Phys 106:9213
28. Rust M, Lappe J, Cave RJ (2002) J Phys Chem A 106:3930
29. (a) Werner H-J, Meyer W (1981) J Chem Phys 74:5802; (b) Macias A, Riera A (1978) J Phys B 11:L489
30. Nakamura H, Truhlar DG (2001) J Chem Phys 115:10353
31. Cave RJ, Newton MD, Kumar K, Zimmt MB (1995) J Phys Chem 99:17501
32. Brunschwig BS, Creutz C, Sutin N (1998) Coord Chem Rev 177:61
33. Bixon M, Jortner J, Verhoeven JW (1994) J Am Chem Soc 116:7349
34. Van Dantzig NA, Levy DH, Vigo C, Piotrowiak P (1995) J Chem Phys 103:4894
35. Newton MD (1991) Chem Rev 91:767
36. McConnell HM (1961) J Chem Phys 35:508
37. Liang CX, Newton MD (1993) J Chem Phys 97:3199
38. Newton MD, Cave RJ (1997) In: Jortner J, Ratner MA (eds), Molecular electronics. Blackwell, Oxford, pp 73–118
39. Newton MD (1999) Adv Chem Phys 106:303
40. Curtiss LA, Naleway CA, Miller JR (1993) Chem Phys 176:387
41. Shepard MJ, Paddon-Row MN, Jordan KD (1993) Chem Phys 176:289
42. Jordan KD, Paddon-Row MN (1992) Chem Rev 92:395
43. Newton MD (2000) Int J Quantum Chem 77:255
44. Zerner MC, Loew GH, Kirchner RF, Mueller-Westerhoff UT (1980) J Am Chem Soc 102:589
45. Dewar MJS, Zoebisch EG, Healy EF, Stewart JJP (1985) J Am Chem Soc 107:3902
46. Newton MD (2003) Coord Chem Rev 238:167
47. Newton MD, Ohta K, Zhong E (1991) J Phys Chem 95:2317
48. Baik M-H, Crystal JB, Friesner RA (2002) Inorg Chem 41:5926
49. Smalley JF, Finklea HO, Chidsey CED, Linford MR, Creager SE, Ferraris JP, Chalfant K, Zawodzinsk T, Feldberg SW, Newton MD (2003) J Am Chem Soc 125:2004
50. Smalley JF, Feldberg SW, Chidsey CED, Linford MR, Newton MD, Liu Y-P (1995) J Phys Chem 99:13141
51. Sikes HD, Smalley JF, Dudek SP, Cook AR, Newton MD, Chidsey CED, Feldberg SW (2001) Science 291:1519
52. Newton MD (2003) ACS Symp Ser 844:196
53. Stuchebrukhov AA, Marcus RA (1995) J Phys Chem 99:7581
54. Harrison RM, Brotin T, Noll BC, Michl J (1997) Organometallics 16:3401
55. Sachs SB, Dudek SP, Hsung RP, Sita LR, Smalley JF, Newton MD, Feldberg SW, Chidsey CED (1997) J Am Chem Soc 119:10563
56. Creager S, Yu CJ, Bamdad C, O'Connor S, MacLean T, Lam E, Chong Y, Olsen GT, Luo J, Gozin M, Kayyem JF (1999) J Am Chem Soc 121:1059
57. Smalley JF

58. Seminario JM, Zacarias AG, Tour JM (1998) J Am Chem Soc 120:3970
59. Davis WB, Svec WA, Ratner MA, Wasielewski MR (1998) Nature 396:60
60. Kuznetsov AM (1981) Nouv J Chem 8/9:427
61. Hayashi S, Kato S (1998) J Phys Chem A 102:3333
62. Liu Y-P, Newton MD (1995) J Phys Chem 99:12382
63. Jonker SA, Ariese F, Verhoeven JW (1989) Recl Trav Chim Pays-Bas 108:109
64. (a) Jones G II, Farahat MS, Greenfield SR, Gosztola DJ, Wasielewski MR (1994) Chem Phys Lett 229:40; (b) Jones G II, Yan D-X, Greenfield SR, Gosztola DJ, Wasielewski MR (1997) J Phys Chem A 101:4939
65. Lappe J, Cave RJ, Jones G, Newton MD, Rostov IV (to be published)
66. Rappe AK, Casewit CJ, Colwell KS, Goddard WA III, Skiff WM (1992) J Am Chem Soc 114:10024
67. Basilevsky MV, Rostov IV, Newton MD (1998) J Electroanal Chem 450:69
68. Tomasi J, Persico M (1994) Chem Rev 94:2027
69. Basilevsky MV, Rostov IV, Newton MD (1998) Chem Phys 232:189
70. Kim HJ, Hynes JT (1992) J Chem Phys 96:5088
71. Goubitz K, Reiss CA, Heijdenrijk, Jonker SA, Verhoeven JW (1989) Acta Crystallogr Sect C45:1348
72. Kuznetsov AM, Ulstrup J (1981) J Chem Phys 75:2047
73. Hayashi S, Kato S (1998) J Phys Chem A 102:3333
74. Lewis FD, Letsinger RL, Wasielewski MR (2001) Acc Chem Res 34:159
75. Jortner J (1976) J Chem Phys 64:4860
76. (a) Cho M, Silbey RJ (1995) J Chem Phys 103:595; (b) Tang J, Norris JR (1994) J Chem Phys 101:5615; (c) Hilczer M, Tachiya M (1996) J Phys Chem 100:8815; (d) Marchi M, Gehlen JN, Chandler D, Newton MD (1993) 115:4178
77. Liu Y-P, Newton MD (1994) J Phys Chem 98:7162
78. Tong GSM, Kurnikov IV, Beratan DN (2002) J Phys Chem B 106:2381
79. (a) Tavernier HL, Fayer MD (2000) J Phys Chem B 104:11541; (b) Siriwong K, Voityuk AA, Newton MD, Rosch N (2003) J Phys Chem B107:2595
80. Yang L, Weerasinghe S, Smith PE, Pettitt BM (1995) Biophys J 69:1519
81. Young MA, Jayaram B, Beveridge DL (1998) J Phys Chem B 102:7666
82. Daizadeh I, Medvedev ES, Stuchebrukhov (1997) Proc Nat Acad Sci USA 94:3703
83. Skourtis SS, Archontis G, Xie Q (2001) J Chem Phys 115:9444
84. Balabin IA, Onuchic JN (2000) Science 290:114
85. Jones GA, Paddon-Row MN, Carpenter BK, Piotrowiak P (2002) J Phys Chem A 106:5011
86. Ribou A-C, Launay J-P, Sachtleben ML, Li H, Spangler CW (1996) Inorg Chem 35:3735
87. Woitellier S, Launay JP, Spangler CW (1989) Inorg Chem 28:758
88. (a) Reimers JR, Hush NS (1990) Inorg Chem 29:3686; (b) Reimers JR, Hush NS (1990) Inorg Chem 29:4510